

Multiple Solid Forms of 1,5-Bis(salicylidene)carbohydrazide: Polymorph-Modulated Thermal Reactivity

Mirta Rubčić,^{*,†} Nives Galić,^{*,†} Ivan Halasz,[‡] Tomislav Jednačak,[†] Nenad Judaš,[†] Janez Plavec,[§] Primož Šket,[§] and Predrag Novak[†]

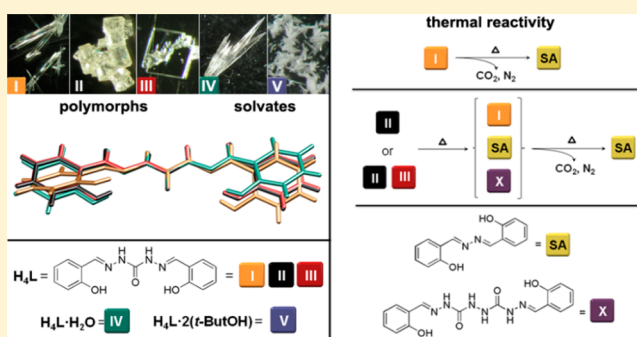
[†]Department of Chemistry, Faculty of Science, University of Zagreb, Horvatovac 102a, HR-10000 Zagreb, Croatia

[‡]Ruder Bošković Institute, Bijenička 54, HR-10000 Zagreb, Croatia

[§]NMR Center, National Institute of Chemistry, SI-1000 Ljubljana, Slovenia

S Supporting Information

ABSTRACT: 1,5-Bis(salicylidene)carbohydrazide, prepared by a condensation reaction of salicylaldehyde and carbohydrazide, afforded a diversity of crystalline forms depending on crystallization conditions: three polymorphs (I, II, and III) and two solvates (IV and V). All solid phases comprise the same tautomer of the title compound, which bears the salicylidene residues in the enol-imino form and the carbamide fragment in the keto form, as established via X-ray crystallography, IR spectroscopy, and cross-polarization magic-angle spinning (CP MAS) NMR (¹³C and ¹H). Conformations of 1,5-bis(salicylidene)carbohydrazide molecules and their hydrogen-bonding patterns are similar for two polymorphs (II and III), while the third one (I) in this context differs significantly. Thermal analyses revealed that all phases undergo complicated degradation upon heating, yielding salicylideneazine, CO₂, and N₂ either directly or via intermediates. Relative phase stability was inspected mechanochemically and by solvent-mediated experiments, establishing polymorph II as the stable one at ambient conditions. NMR and UV–visible solution studies revealed that the same tautomer of 1,5-bis(salicylidene)carbohydrazide present in the solid state is also the dominant one in solution.



INTRODUCTION

Carbohydrazide and its derivatives have been investigated since 1894 when their syntheses were first reported.¹ Initially they were used as precursors for the syntheses of various nitrogen-containing heterocyclic compounds,² while later they came into focus for their biological properties³ as well as their reactivity, which led to notable industrial applications.⁴ As a higher urea homologue, carbohydrazide offers wide possibilities for tailoring imino compounds (mono- and bis-substituted, symmetrical and asymmetrical), which are progressively recognized not only as chelating agents but also as functional molecules, for example, for selective anion binding.⁵ While most of the older work on carbohydrazide Schiff bases focused on their applicability in classical analysis,⁶ nowadays these systems are increasingly acknowledged as supreme multitopic ligands for the targeted construction of extended metal–organic architectures.⁷

The occurrence of multiple distinct solid forms—that is, polymorphs, solvates, and amorphous phases—for a given compound and control over their formation has been a vital topic in the field of solid-state chemistry for more than a century now.⁸ Reasons for that are numerous, but the most significant relate to the fact that different solid forms may differ dramatically in their physicochemical properties (thermal behavior, stability, solubility, bioavailability, etc.).⁹ Polymorph

ism in particular manifests the variety in organization of structural units within a crystal through different intermolecular bonding patterns and/or by conformational adaptations.^{8e,10} Naturally, the more profound these differences are, the more diverse properties can be expected, as exemplified by dissimilar photochemical reactivity of polymorphs of *trans*-cinnamic acid.¹¹ The phenomenon of multiple solids thus stretches far beyond purely academic fascination as its overlooking can have consequences in the production and commercialization of solid materials, for example, in the industries of dyes and pigments and explosives,^{8e,12} as well as in the pharmaceutical industry, where this was astonishingly demonstrated by the case of the drug ritonavir.¹³

Herein we present a comprehensive solid-state and solution study of a Schiff base derived from carbohydrazide and salicylaldehyde. Namely, we portray five crystalline forms of 1,5-bis(salicylidene)carbohydrazide, three of which are polymorphs and the remaining two are solvates. The occurrence conditions of all phases were investigated by a variety of synthetic and crystallization procedures including also solvent-

Received: February 9, 2014

Revised: April 8, 2014

Published: April 9, 2014

free routes. Relative stabilities of the isolated forms and their (inter)conversions were inspected through a number of solution and solid-state experiments. Particularly interesting results were obtained via thermal analyses revealing complicated and polymorph-dependent degradation scenarios for these compounds.

EXPERIMENTAL SECTION

Materials. Carbohydrazide (minimum 98%) and salicylaldehyde (minimum 98%) were purchased from Sigma–Aldrich (St. Louis, MO) and used as received. Solvents used in syntheses or recrystallization experiments (p.a. grade) were purchased from Kemika (Zagreb, Croatia) and were distilled before use. For spectrophotometric measurements, solvents of spectrophotometric grade were chosen (purchased from Kemika) and were used without further purification.

Synthesis of 1,5-Bis(salicylidene)carbohydrazide, H₄L (Polymorphs I, II, and III). Carbohydrazide (0.20 g, 2.22 mmol) was stirred and heated in methanol (10 mL) until it was completely dissolved. Methanolic solution of salicylaldehyde (0.54 g, 4.44 mmol of salicylaldehyde in 2 mL of MeOH) was then added to a carbohydrazide solution, and depending on the subsequent heating and stirring regime, two polymorphs, I and II, were obtained as pure phases. If the reaction mixture was stirred and vigorously heated within 1 h, colorless needlelike product I emerged (Figure 1). In contrast, if

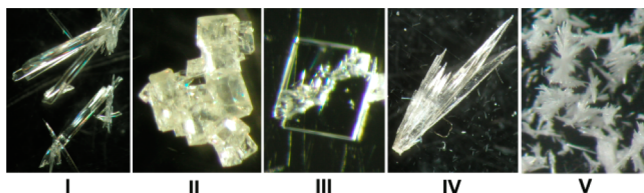


Figure 1. Crystals of 1,5-bis(salicylidene)carbohydrazide polymorphs (I, II, and III), 1,5-bis(salicylidene)carbohydrazide monohydrate (IV), and 1,5-bis(salicylidene)carbohydrazide di(*tert*-butanol) solvate (V).

the reaction mixture was not stirred and was gently warmed (ca. 40 °C), polymorph II, in the form of beige prisms, was harvested (Figure 1). In both cases, reaction mixtures were heated/stirred for 3 h total. Mother liquors of both reaction mixtures yielded first prisms of II and then, after about a week, thin, colorless plates of III (Figure 1). However, III appeared always concomitantly with II (often intergrown), and due to their morphological similarity (when their crystal faces were not well developed) they could not be differentiated. Consequently, crystals of II and III could not be separated manually.

Polymorph I: yield 0.53 g (80%). Anal. Calcd for C₁₅H₁₄N₄O₃: C, 60.40; H, 4.73; N, 18.79. Found: C, 60.5; H, 4.7; N, 18.6. IR (KBr, cm⁻¹) 1651 ($\nu_{C=O}$), 1618 ($\nu_{C=N}$), 1572 ($\nu_{C=C}$), 1486 (δ_{N-H}), 1274 ($\nu_{C(O)-N}$), 1220 (ν_{C-O}).

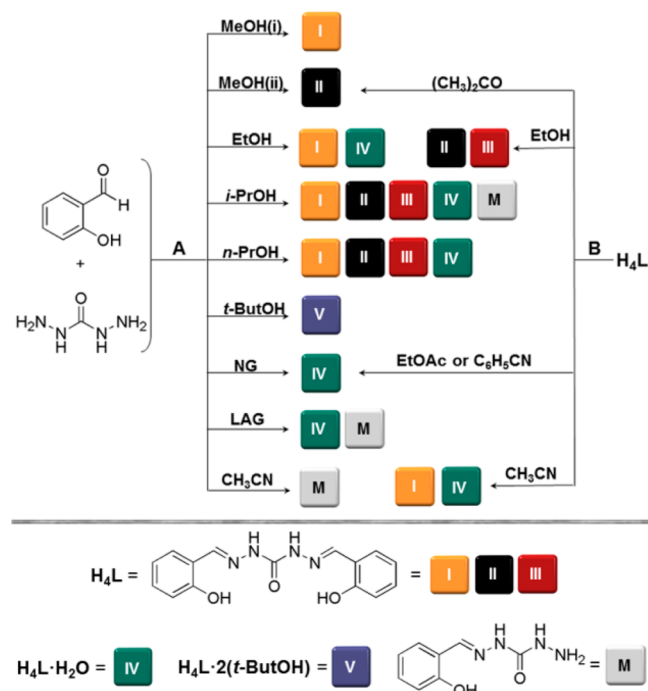
Polymorph II: yield 0.55 g (83%). Anal. Calcd for C₁₅H₁₄N₄O₃: C, 60.40; H, 4.73; N, 18.79. Found: C, 60.3; H, 4.7; N, 18.8. IR (KBr, cm⁻¹) 1715 ($\nu_{C=O}$), 1609 ($\nu_{C=N}$), 1551 ($\nu_{C=C}$), 1491 (δ_{N-H}), 1266 ($\nu_{C(O)-N}$), 1211 (ν_{C-O}).

Polymorph II/III mixture: Anal. Calcd for C₁₅H₁₄N₄O₃: C, 60.40; H, 4.73; N, 18.79. Found: C, 60.3; H, 4.8; N, 18.6. IR (KBr, cm⁻¹) 1714 ($\nu_{C=O}$), 1622 ($\nu_{C=N}$), 1551 ($\nu_{C=C}$), 1489 (δ_{N-H}), 1269 ($\nu_{C(O)-N}$), 1210 (ν_{C-O}).

All isolated phases were analyzed via PXRD (powder X-ray diffraction) and the collected patterns were compared with those simulated from SCXRD (single-crystal X-ray diffraction) data (Figures S1 and S2, Supporting Information). Pure I can be also obtained by heating IV and V to 180 °C (vide infra). Crystals of I of satisfying quality for diffraction experiments were obtained by the synthesis in methanol using 4,4'-bipy as an additive (carbohydrazide 1.11 mmol, salicylaldehyde 2.22 mmol, 4,4'-bipy 11.1 mmol, 20 mL of methanol) (Figure S3, Supporting Information).¹⁴

Reaction of Salicylaldehyde and Carbohydrazide (2:1) in Acetonitrile. Carbohydrazide (0.10 g, 1.11 mmol) was stirred and heated in acetonitrile (17 mL) until it was completely dissolved. Afterward, acetonitrile solution of salicylaldehyde (0.27 g, 2.22 mmol of salicylaldehyde in 3 mL of CH₃CN) was added to a carbohydrazide solution. Regardless of the subsequent heating/stirring regime (gentle warming without stirring or vigorous stirring and heating for 3 h total), the same product, salicylidene carbohydrazide (M), was obtained as a white precipitate (Scheme 1), yield 0.12–0.13 g (36–40%). The material was identified as M via PXRD analysis (Figure S4, Supporting Information).

Scheme 1. Occurrence Conditions for Forms I–V of 1,5-Bis(salicylidene)carbohydrazide and Monosubstitutes Derivative M^a



^a(A) Synthesis (molar ratio 2:1); (B) recrystallization. NG, neat grinding; LAG, liquid-assisted grinding, performed with methanol (MeOH) or acetonitrile (CH₃CN); MeOH(i), synthesis in methanol (stirring and heating at boiling point); MeOH(ii), synthesis in methanol (no stirring and mild heating); EtOH, ethanol; EtOAc, ethyl acetate; *n*-PrOH, 1-propanol; *i*-PrOH, 2-propanol; *t*-ButOH, *t*-butanol; (CH₃)₂CO, acetone; C₆H₅CN, benzonitrile.

Synthesis of 1,5-Bis(salicylidene)carbohydrazide Monohydrate, H₄L·H₂O (IV). Although this form appeared on prolonged standing (several weeks) from methanolic (Figure S1e, Supporting Information), ethanolic, 1-propanolic, 2-propanolic, and acetonitrile mother liquors, pure IV was obtained by grinding carbohydrazide (0.05 g, 0.56 mmol) with salicylaldehyde (120 μ L, 1.13 mmol) for 40 min (Figure S5, Supporting Information), or by grinding I, II, or II/III mixture (about 150 mg) with 1 drop of water for 40 min (Figure S6, Supporting Information). Yields of IV obtained by these procedures were nearly 100%. Pure form IV was also obtained by recrystallization from benzonitrile or ethyl acetate (Figure S7b,c, Supporting Information). IV. Anal. Calcd for C₁₅H₁₆N₄O₄: C, 56.95; H, 5.10; N, 17.72. Found: C, 56.7; H, 4.9; N, 17.7. IR (KBr, cm⁻¹) 1683 ($\nu_{C=O}$), 1621 ($\nu_{C=N}$), 1583 ($\nu_{C=C}$), 1491 (δ_{N-H}), 1270 ($\nu_{C(O)-N}$), 1219 (ν_{C-O}).

Liquid-Assisted Grinding of Salicylaldehyde and Carbohydrazide. Salicylaldehyde (120 μ L, 1.13 mmol) and carbohydrazide (0.05 g, 0.56 mmol) were ground for 40 min with the addition of 1 drop of acetonitrile or methanol. The composition of the material was

established via PXRD analysis as a mixture of IV and M (Figure S8, Supporting Information).

Reaction of Salicylaldehyde and Carbohydrazide (2:1) in Ethanol, 1-Propanol, and 2-Propanol. Carbohydrazide (0.10 g, 1.11 mmol) was stirred and heated in ethanol (10 mL) until it was completely dissolved. Afterward, ethanolic solution of salicylaldehyde (0.27 g, 2.22 mmol of salicylaldehyde in 2 mL of EtOH) was added to a carbohydrazide solution and the reaction mixture was heated without stirring (ca. 50 °C). Within 5–10 min after the addition of salicylaldehyde, white product started to deposit. Heating was continued for 3 h and the obtained material was filtered off, washed with a small amount of cold ethanol, and dried in air (yield 0.20 g). The composition of the material was established via PXRD analysis as a mixture of phases I and IV (Figure S9a, Supporting Information). In attempt to direct the reaction toward pure phase IV, synthesis was conducted in a similar way but with the addition of 2 or 3 drops of water. However, this has not influenced the crystallization outcome since again mixture of phases I and IV was isolated. Mother liquors yielded, just as in the case of methanol, II/III mixture (Figure S7a, Supporting Information).

Reactions in 1-propanol and 2-propanol were performed in a similar way as that in ethanol, with 0.10 g of carbohydrazide (1.11 mmol), 0.27 g of salicylaldehyde (2.22 mmol), and 12 mL of *n*-PrOH or 16 mL of *i*-PrOH. Reaction mixtures were heated (ca. 50 °C) without stirring for 3 h, during which white material deposited (in the case of *i*-PrOH, precipitate started to form after 5 min). The precipitates were filtered off, washed with a small amount of cold alcohol, and dried in air (yield 0.22 g from *n*-PrOH, 0.23 g from *i*-PrOH). The composition of the obtained materials was established via PXRD analysis as a mixture of phases I, II, III, and IV (*n*-PrOH) and as a mixture of I, II, III, IV, and M (*i*-PrOH) (Figure S9b,c, Supporting Information).

Synthesis of 1,5-Bis(salicylidene)carbohydrazone Di(*tert*-butanol) Solvate, H₄L-2(*t*-BuOH) (V). Carbohydrazide (0.10 g, 1.11 mmol) was stirred and heated in *tert*-butanol (10 mL) until complete dissolution. *tert*-Butanol solution of salicylaldehyde (0.27 g, 2.22 mmol of salicylaldehyde in 3 mL of *t*-BuOH) was added to a carbohydrazide solution, and the reaction mixture was afterward heated (ca. 50 °C) for 3 h. During this period, colorless needlelike crystals of V slowly formed (Figure 1; Figure S1f, Supporting Information). Yield 0.30 g (60%). Anal. Calcd for C₂₃H₃₄N₄O₅: C, 61.86; H, 7.68; N, 12.55. Found: C, 62.0; H, 7.6; N, 12.4. IR (KBr, cm⁻¹) 1683 ($\nu_{C=O}$), 1622 ($\nu_{C=N}$), 1587 ($\nu_{C=C}$), 1490 (δ_{N-H}), 1273 ($\nu_{C(O)-N}$), 1217 (ν_{C-O}). Upon longer air exposure (ca. 2 weeks), V transforms to a mixture of I and IV (Figure S10, Supporting Information).

Recrystallization of H₄L from EtOH. Recrystallization outcomes were inspected for solutions in the concentration range between 1 and 10 mmol·dm⁻³. In all cases a mixture of forms II and III was obtained (Figure S7a, Supporting Information). Crystallization outcome did not depend on the initial phase used (I or II).

Also, it should be noted that in all procedures described thus far, mother liquors were kept in flasks tightly closed with rubber stoppers, thus not allowing significant solvent evaporation.

Recrystallization of H₄L from Acetonitrile, Benzonitrile, Ethyl Acetate, and Acetone. H₄L (0.20 g, I or II) was dissolved (with heating) in the following solvent volumes: 5 mL (acetone), 5 mL (acetonitrile), 10 mL (ethyl acetate), and 3 mL (benzonitrile). The corresponding solutions were kept in test tubes closed with parafilm. Within 1 day, in all cases, crystalline materials deposited. The composition of the obtained solids was established via PXRD analysis as follows: II from acetone, IV from ethyl acetate and benzonitrile, and a mixture of I and IV from acetonitrile (Figure S7b–e, Supporting Information).

Solvent-Mediated Experiments. Altogether five experiments were performed at room temperature. In each, a slurry of a mixture of selected forms in methanolic mother liquor (left after the isolation of I) was prepared. In the first experiment a mixture of I and II was investigated; in the second a mixture of II and III; in the third a mixture of I, II, and III; in the fourth a mixture of I, II, III, and IV; and in the fifth a mixture of I, II, III, IV, and V. The precipitates were

sampled at regular intervals and complete conversion to II was established after 4 h for the mixture of I and II; after 6 h for the mixture of II and III; after 21 h for the mixture of I, II, and III; after 6 h for the mixture of I, II, III, and IV; and after 32 h for the mixture of I, II, III, IV, and V (Figure S11, Supporting Information).

Methods. Elemental analyses (C, H, N) were provided by the Analytical Services Laboratory of the Rudjer Bošković Institute, Zagreb, Croatia. Powder patterns (used for qualitative analysis) of the samples were collected on a Philips PW 3710 diffractometer, Cu K α radiation, flat plate sample on a zero background in Bragg–Brentano geometry, tension 40 kV, current 40 mA. The patterns were collected in the angle region between 4° and 40(50)° (2 θ) with a step size of 0.02° and 1.0 s counting/step. Neat grinding (NG) and liquid-assisted grinding (LAG) were performed with a Retsch MM200 ball mill (25 Hz) for 40 min. After such treatment, PXRD patterns were collected for all samples. IR spectra (KBr pellets) were recorded on a Bruker Vector 22 spectrometer. The number of scans accumulated for each spectrum was 20 at a spectral resolution of 4 cm⁻¹ in the range between 4000 and 400 cm⁻¹. Thermogravimetric analyses (TGA) were performed on a Mettler-Toledo TGA/SDTA851e thermobalance with aluminum crucibles under nitrogen stream, with the heating rate depending on the experiment (5 or 1 °C·min⁻¹). The results were processed with the Mettler STARe 9.01 software. Differential scanning calorimetry (DSC) measurements were performed under the nitrogen stream on the Mettler–Toledo DSC823e calorimeter with STARe SW 9.01 (heating rate depended on the experiment, 5 or 1 °C·min⁻¹). Temperature-resolved powder X-ray diffraction (TR-PXRD) measurements were performed on the Bruker D8 Advance in Debye–Scherrer geometry with V α ntag-1 position-sensitive detector with a 6° opening angle and Cu K α 1 radiation from primary Ge(111)-Johansson-type monochromator, equipped with a capillary furnace (mri Physikalisches Geräte GmbH). The sample was placed in a 0.5 mm borosilicate glass capillary. Data collection of each pattern was set to start after the desired temperature was reached, which was then held constant during the data collection of each pattern. A heating rate of 0.5 °C·s⁻¹ was used and data were collected over 30 min for each pattern in all in situ heating experiments. Patterns were collected in the 2 θ region of 5–35.8. The ESI mass spectra were obtained on an Agilent 6410 triple quadrupole mass spectrometer. Mass spectra were recorded in the range of m/z = 100–2000 in positive and negative ion modes. Capillary potential was 4 kV and fragmentor voltage was 135 V. Gas temperature was 350 °C and gas flow rate was 12 dm³·min. Samples were introduced into the mass spectrometer directly via Agilent 1260 HPLC (Agilent Technologies, Palo Alto, CA) by infusion. Solid-state NMR spectra of forms I–V were recorded on a Varian NMR system 600 MHz NMR spectrometer equipped with 1.6 mm fast magic-angle spinning (MAS) solids probe. Larmor frequencies of protons and carbon nuclei were 599.65 and 150.78 MHz. The ¹H MAS NMR spectra were externally referenced to adamantane. The ¹³C cross-polarization (CP) MAS NMR spectra were externally referenced to glycine. All samples were spun at the magic angle with 20 kHz during ¹H measurements and 16 kHz during ¹³C measurements. The proton spectra were acquired by use of a spin–echo sequence. Repetition delay was 5 s. The number of scans was 16. The pulse sequence used for acquiring the carbon spectra was a standard cross-polarization MAS pulse sequence with high-power proton decoupling during acquisition. Repetition delay was 5 s and the number of scans was between 600 and 1600, depending on the sample. Solution-state NMR spectra were recorded on a Bruker Avance 600 spectrometer equipped with an inverse probe and z -gradient accessories and operating at constant magnetic field of 14.2 T. Samples were measured in 5 mm tubes at 298 K with dimethyl sulfoxide (DMSO) as a solvent and tetramethylsilane (TMS) as an internal standard. For other specific measurement details, see Supporting Information. UV–vis spectra were acquired by means of a Varian Cary 3 spectrometer in the spectral range 200–500 nm. Conventional quartz cells (l = 1 cm) were used throughout.

Single-Crystal X-ray Diffraction Experiments. Selected crystallographic and refinement data for structures I, II, III and IV, obtained by single-crystal X-ray diffraction, are reported in Table S1 (Supporting Information). The data for all structures were collected at

295 K on an Oxford Xcalibur diffractometer equipped with 4-circle κ geometry goniometer, charge-coupled device (CCD) Sapphire 3 detector, and graphite-monochromated Mo $K\alpha$ radiation ($\lambda = 0.71073$ Å) via ω -scans. Data reduction, including that performed on a twinned data set (III), and empirical absorption correction were done with the CrysAlis software package.¹⁵ Structures were solved by direct methods and refined against F^2 by a weighted full-matrix least-squares method. Programs SHELXS-97¹⁶ and SHELXL-97¹⁶ integrated in the WinGX¹⁷ software system were used to solve and refine all structures. All non-hydrogen atoms were refined anisotropically. Hydrogen atoms bound to carbon atoms were placed in geometrically idealized positions and refined by use of the riding model. Hydrogen atoms attached to amino N1 (and N3) and phenolic O1 (and O3) atoms, and for IV water OW atoms, were located in the difference Fourier maps at the final stages of the refinement procedure. Their coordinates were refined freely but with restrained N–H and O–H distances of 0.86 and 0.82 Å, respectively. For the structures of II and IV, which crystallize in noncentrosymmetric space groups (*Aba2* and *C22₁*, respectively) due to the absence of significant anomalous scattering, Friedel pairs were merged and the absolute structure was assigned arbitrarily. For the structure of III, careful inspection of its reciprocal space, via Ewald explorer, revealed the case of nonmerohedral twinning. Lattices of the two twin components were clearly visible and were indexed manually. The twin law was found to correspond to a 2-fold rotation around the *a* axis, that is, (1 0 0/0 –1 0/–0.6529 0 –1). Decomposition of the twinned data set revealed that the two twin domains are present in the ratio 0.48:0.52. Overall 1667 reflections were isolated for the first domain and 1646 for the second one, leaving 2503 overlapped reflections. The structure was solved with detwinned hklf4 file of the major twin component and refined with the twinned hklf5 file containing merged data. Geometrical calculations and structural analyses were conducted with PLATON¹⁸ and PARST.¹⁹ Drawings were made with ORTEP-3,²⁰ POV-Ray,²¹ and Mercury.²² Main geometrical features (selected bond distances and angles) along with hydrogen-bond geometry for all examined structures are given in Table 1 and Table S2 (Supporting Information).

RESULTS

Syntheses. The synthesis of bis(salicylidene)-carbohydrazide (H_4L), and independently the crystal structure of its hydrate form ($H_4L \cdot H_2O$), were first published in the mid-1980s.²³ None of the accounts that followed, which described the synthesis of the H_4L (all declared as nonsolvates) in several different ways, reported on the compound's polymorphism,²⁴ although some of the data presented therein, in particular IR spectra and melting point data, were rather inconsistent. Only recently, the structure of one of its anhydro forms (here named II) was elucidated but without detailed description of its synthesis or solid-state properties.²⁵ Since we detected, even during preliminary synthesis, two distinct solid phases of H_4L (both nonsolvates), it intrigued us to explore this system more closely.²⁶

Reaction of salicylaldehyde (sal) and carbohydrazide (chdr) in methanol in the molar ratio 2:1 under vigorous stirring and heating at the boiling point yielded colorless needlelike crystals of H_4L , here regarded as form I (Figure 1; Figures S1 and S2 in Supporting Information; Scheme 1). In contrast, when the reaction was conducted in the same solvent but was only gently warmed (ca. 40 °C) without stirring, pale yellow prisms of the second polymorphic phase of H_4L , form II, emerged (Figure 1; Figures S1 and S2 in Supporting Information; Scheme 1). The remaining mother liquors, in both cases, yielded after about a week concomitantly with II small quantities of very thin colorless plates, identified via single-crystal X-ray diffraction (SCXRD) as the third polymorph of H_4L , phase III (Figure 1; Figures S1, S2, and S7a in Supporting Information). On the

other hand, if the mother liquors were allowed to stand for several weeks, II/III mixture slowly dissolved to produce the previously reported hydrate form $H_4L \cdot H_2O$, here named as IV (Figure 1; Figures S1 and S2 in Supporting Information). Although four forms were harvested from only one solvent, two problems remained. First, III appeared always concomitantly and often intergrown with crystals of II, making it impossible to obtain this phase pure in larger quantities. Second, the only route to IV was at that point prolonged standing of mother liquids, which again yielded this compound in hardly satisfying quantities. To define thus more properly the occurrence domains for the detected phases, in particular III and IV, we inspected the influence of different solvents on the reaction and/or recrystallization outcome.

The reaction of sal and chdr (2:1) in acetonitrile, regardless of heating/stirring regime, yielded a white product, identified as the recently reported monosubstituted derivative of carbohydrazide (M) (Scheme 1; Figure S4 in Supporting Information).²⁷ Syntheses from ethanol, 2-propanol, and 1-propanol afforded mixtures (Scheme 1; Figure S9 in Supporting Information; for details see Experimental Section), whereas in the case of *tert*-butanol, poor-quality colorless crystals of an entirely new phase were obtained (Figure 1; Figure S1f in Supporting Information). On the basis of chemical analysis, solid-state NMR, and thermal analysis data, these were formulated as di(*tert*-butanol) solvate, $H_4L \cdot 2(t\text{-BuOH})$, or form V (Scheme 1). It is worth noting that, upon longer air exposure (ca. 2 weeks), this compound inevitably transformed to I/IV mixture (Figure S10, Supporting Information). Since ethanolic mother liquors yielded II/III mixture (Figure S7a, Supporting Information), an attempt was made to obtain pure III via recrystallization from ethanol. However, such procedure proved unsuccessful: regardless of the solution's concentration (see Experimental Section), II/III mixtures were harvested exclusively. Recrystallization from aprotic solvents afforded the following phases: IV from benzonitrile and ethyl acetate, II from acetone, and I/IV mixture from acetonitrile (respectively panels b–c, d, and e of Figure S7, Supporting Information). It is worth noting that the recrystallization outcome did not depend on the initial phase used (I or II).

Complementing the solution synthesis, mechanochemical approaches (e.g., neat grinding and LAG) often provide alternative routes to the desired products.²⁸ Here, grinding of sal and chdr (2:1) provided an elegant route to IV; 40 min of grinding afforded this phase pure in quantitative yield (Scheme 1; Figure S5 in Supporting Information). However, a similar LAG approach (with MeOH or CH_3CN) has not proved as successful since only impure materials were obtained, that is, IV with small amounts of M (Scheme 1; Figure S8 in Supporting Information).

Crystal Structures. Forms I–IV crystallize as keto tautomers with respect to the central carbamide fragment (Figure 2; Figure S12 and Table S2 in Supporting Information), while their salicylidene residues adopt the enol-imino tautomeric form characterized by strong intramolecular hydrogen bonds of the O–H \cdots N type (Table 1). H_4L molecules found in II, III, and IV are essentially planar and the difference between their conformations is small, whereas molecules of I appreciably deviate from planarity (Figure 3).

Different conformations in I on one hand and in II and III on the other relate to different supramolecular architectures. Molecules in I associate through N–H \cdots O hydrogen bonds into infinite chains, which extend along the *c*-axis (Figure 4a,

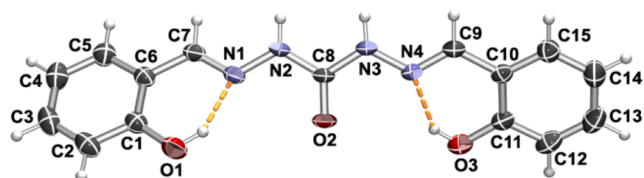


Figure 2. ORTEP²⁰-POV-Ray²¹ rendered view of molecular structure of **I**, with atom-numbering scheme. Displacement ellipsoids are drawn at the 30% probability level. Hydrogen atoms are presented as spheres of arbitrary small radius. Intramolecular hydrogen bonds, O1–H1O...N1 and O3–H3O...N4, are denoted with orange dashed lines. The asymmetric units of **II**, **III** and **IV** contain half of the molecule presented, as in those structures the central C8–O2 fragment lies on a 2-fold rotation axis.

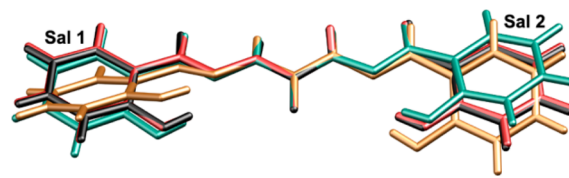


Figure 3. Mercury²²-POV-Ray²¹ rendered view of the overlapping diagram of **I** (orange), **II** (black), **III** (red), and **IV** (green). The diagram was constructed by overlapping atoms of the central carbamide part of the molecules. Dihedral angles between the planes of Sal 1 and Sal 2 rings are 53.60(8)° for **I**, 6.86(11)° for **II**, 5.01(19)° for **III**, and 4.85(17)° for **IV**.

Table 1). Both N–H functionalities of the central carbamide fragment bind to the O2 atom of the neighboring molecule, forming a hydrogen-bonded pattern, $R^1_2(6)$ in graph-set notation. Each chain is further stabilized via C–H...O interactions, while the adjacent supramolecular chains assemble through van der Waals interactions (Figure S13, Supporting Information).

The essentially planar molecules of **II** and **III** hinder the O2 atom from participating in hydrogen bonding. Instead, the N–H functionalities of the carbamide fragment bind to the phenolic oxygen atom of the neighboring molecule, affording the $C^1_1(9)$ motifs (Table 1). Such a hydrogen-bonding pattern allows growth of layers, for **II** in the bc plane (Figure 4b; Figure S14 in Supporting Information) and for **III** in the ab plane (Figure 4c; Figure S15 in Supporting Information). The layers found in **II** and **III** show great resemblance, and in both cases molecules within one layer retain the same orientation. However, the difference between **II** and **III** is found in the packing of these layers. In **II**, the two adjacent layers assemble through C–H... π interactions in a herringbone fashion along the a -axis (Figure S14, Supporting Information). In contrast, layers in **III** run mutually parallel and are stacked down the c -axis through van der Waals interactions (Figure S15, Supporting Information).

In **IV**, water molecules bridge neighboring carbohydrazide molecules. Namely, each water molecule associates three closest H_4L molecules via N–H...O bonds, which form the $R^1_2(6)$ motif, and O–H...O hydrogen bonds with the $C^1_2(4)$ graph-set

pattern (Table 1). Such arrangement subsequently leads to formation of a rather large $R^5_6(16)$ hydrogen-bonding motif and the extension of architecture along both a - and b -axis (Figure 4d; Figure S16 in Supporting Information). Layers formed in such manner are additionally supported by C5–H5...O1 interactions. Finally, neighboring layers associate through van der Waals interactions along the c -axis (Figure S16, Supporting Information).

Solid-State NMR Studies. CP MAS NMR spectroscopy can provide a wealth of information on different solid forms and their mixtures and joined with crystallography is a powerful tool in characterization of solid samples.²⁹ ¹³C solid-state CP MAS spectra of forms **I–V** are shown in Figure 5, together with a solution ¹³C spectrum recorded in DMSO- d_6 , which is discussed in detail later in the text (Table 2).

Solid-state spectra of forms **I–V** show only slight dissimilarities, suggesting that H_4L molecules within these phases assume the same tautomeric form but differ in their conformation and/or their environment (Figure 5). The signals arising from C-1 and C-11 atoms (for numbering of atoms see Figure 2), chemical shifts of which are used for distinguishing between keto-amino and enol-imino tautomeric forms, appear in spectra of **I–V** at ca. 152 ppm. This clearly indicates that salicylidene residues of H_4L in all cases adopt the enol-imino form, since in the case of the keto-amino tautomer these carbons should resonate at ca. 180 ppm.³⁰ On the other hand, chemical shifts assigned to C8 atoms (ca. 157 ppm) demonstrate that the carbamide fragment is in all cases present in its keto form.^{27,29e,31} However, a downfield shift is observed for C8 atom signals in the spectra of **I**, **IV**, and **V**, which

Table 1. Geometry of Hydrogen Bonds for Forms **I–IV**

D–H...A	D–H (Å)	H...A (Å)	D...A (Å)	\angle D–H...A (deg)	symmetry code
Form I					
O1–H1O...N1	0.840(17)	1.874(18)	2.5879(15)	142.0(16)	
O3–H3O...N4	0.846(17)	1.921(18)	2.6490(16)	143.5(15)	
N2–H2N...O2	0.833(13)	1.999(13)	2.7630(14)	152.2(14)	$x, 1/2 - y, -1/2 + z$
N3–H3N...O2	0.820(13)	2.119(13)	2.8422(13)	147.0(13)	$x, 1/2 - y, -1/2 + z$
Form II					
O1–H1O...N1	0.83(2)	1.84(3)	2.571(3)	146(3)	
N2–H2N...O1	0.86(2)	2.23(3)	3.020(3)	154(3)	$1 - x, 1/2 - y, 1/2 + z$
Form III					
O1–H1O...N1	0.83(3)	1.88(3)	2.585(4)	142(3)	
N2–H2N...O1	0.85(2)	2.23(2)	3.046(4)	161(2)	$1/2 - x, -1/2 + y, 1/2 - z$
Form IV					
OW–HOW...O2	0.83(2)	1.92(2)	2.743(2)	177(2)	$1/2 + x, 1/2 + y, z$
O1–H1O...N1	0.82(4)	1.93(4)	2.658(4)	146(3)	
N2–H2N...OW	0.86(2)	2.06(2)	2.827(3)	149(3)	

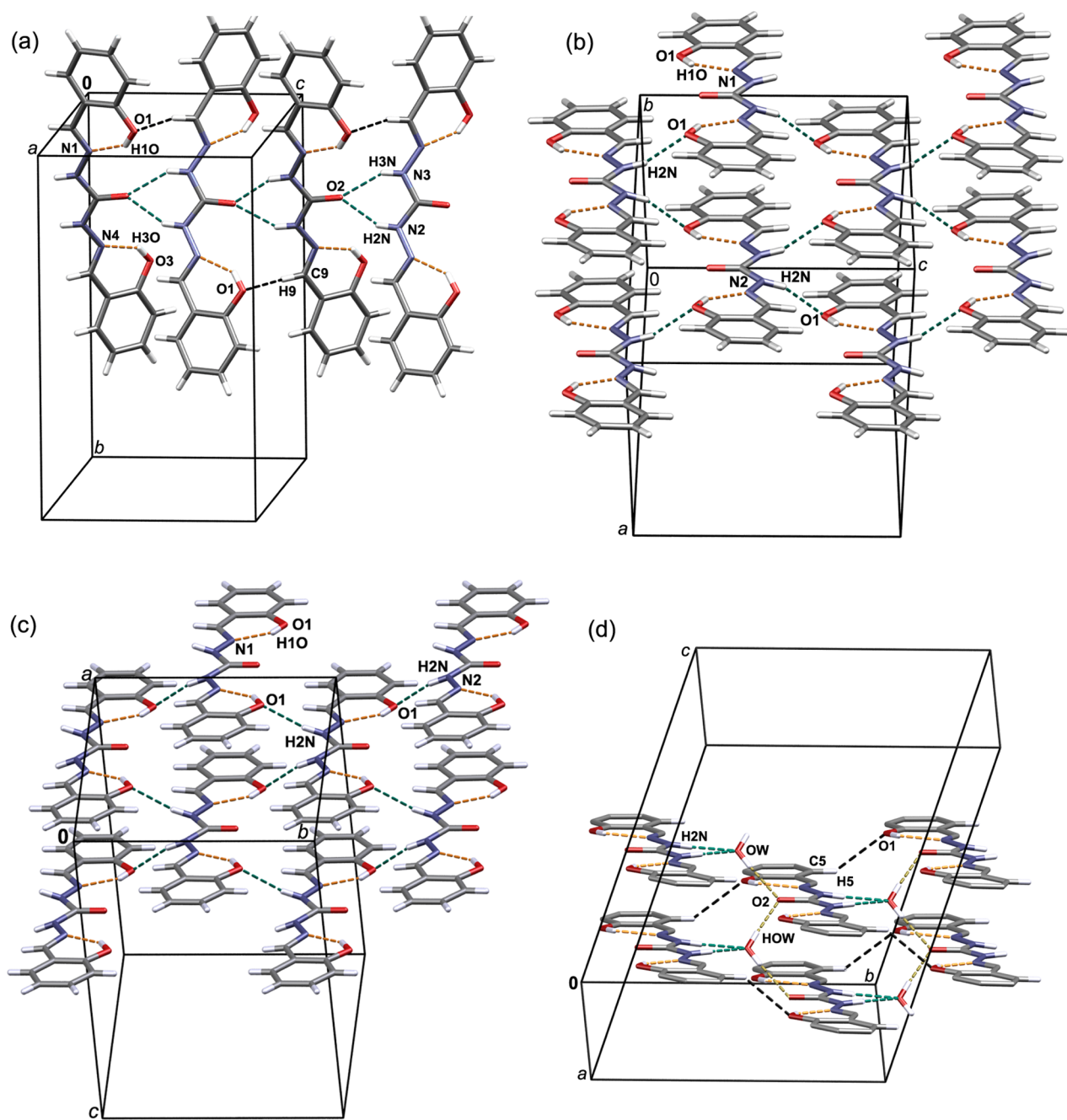


Figure 4. Primary supramolecular architectures in I, II, III, and IV. (a) Infinite one-dimensional supramolecular chain in I spreads along the *c*-axis. Chains are assembled via N–H...O hydrogen bonds (presented by green dashed lines) and C9–H9...O1 interactions (presented by black dashed lines). Main geometrical parameters for C9–H9...O1ⁱ interaction are C9–H9 0.93 Å, H9...O1 2.606(1) Å, C9...O1 3.434(2) Å, ∠C9–H9...O1 148.58(9)°, and $i = x, 1/2 - y, -1/2 + z$. (b) Molecular layer in II forms in the *bc* plane. Layers are associated via N2–H2N...O1 hydrogen bonds (presented by green dashed lines). (c) Molecular layer in III forms in the *ab* plane. Layers are assembled via N2–H2N...O1 hydrogen bonds (presented by green dashed lines). (d) Part of the layer in IV containing water and bis(salicylidene)carbohydrazone molecules which associate through N–H...O and O–H...O hydrogen bonds (presented by green and yellow dashed lines, respectively). Layers are additionally supported by C5–H5...O1 interactions (presented by black dashed lines). Main geometrical parameters for C5–H5...O1ⁱ interaction are C5–H5 0.93 Å, H5...O1 2.5900 Å, C5...O1 3.388(4) Å, ∠C5–H5...O1 144.00°, and $i = 1/2 + x, 1/2 + y, z$. For clarity, in (d), only those hydrogen atoms involved in hydrogen bonding are presented. Intramolecular O–H...N hydrogen bonds are presented by orange dashed lines.

indicates engagement of their central carbonyl moiety in hydrogen bonding.^{29e,31b} In this context, it is important to note that chemical shifts assigned to OH and NH protons for forms II and III, in comparison to other forms, are shifted downfield (¹H CP MAS; Figure S17, Supporting Information). Taken together, these results strongly support structure models of forms I–IV derived from SCXRD data but also provide

valuable insight on the solid-state structure of V. Finally, the signals observed in the ¹³C CP MAS spectrum of V (ca. 70 and 30 ppm) belong to carbon atoms of *tert*-butanol (Figure 5).

IR Spectroscopy. The solid-state structure of each form of H₄L was inspected via IR spectroscopy (Figure 6). Since III could not be separated from II, an IR spectrum of the mixture of polymorphs II/III was recorded and analyzed.

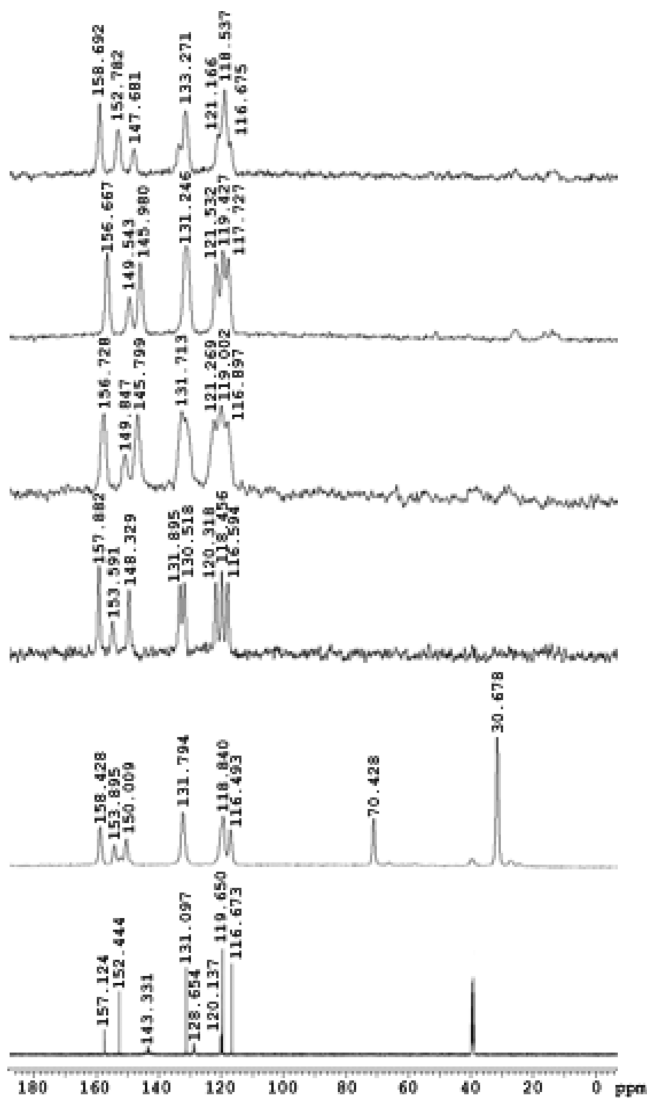


Figure 5. ^{13}C CP-MAS spectra of I, II, II/III mixture, IV, V, and ^{13}C spectra of H_4L in $\text{DMSO}-d_6$ solution (from top to bottom).

Forms I–V display several overlapped bands in the spectral region $3500\text{--}3100\text{ cm}^{-1}$, corresponding to the stretching vibrations of N–H and O–H groups (Figure S18, Supporting Information).^{6a,24a,31a,32} Broadness of these bands indicates engagement of N–H/O–H functionalities in hydrogen bonding in the solid state, while their pattern remains unique for each phase. Spectra of I–V exhibit weak absorption bands at ca. 3050 cm^{-1} arising from the aromatic C–H stretching vibration, whereas the spectrum of V shows an additional prominent band at ca. 2900 cm^{-1} that can be assigned to the C–H vibrations of *tert*-butanol molecule (Figure S18, Supporting Information). However, the most evident differences between the five forms are observed in the spectral region $1750\text{--}1500\text{ cm}^{-1}$, that is, the part characteristic for the C=O stretching vibration (Figure 6). This band (amide I band) for forms II and III appears at considerably higher wavenumbers (1715 and 1714 cm^{-1} , respectively) than in the spectra of the remaining forms. This again strongly supports X-ray diffraction and solid-state NMR data, confirming that in II and III, in contrast to other forms, the central carbonyl moiety does not participate in hydrogen bonding. In all inspected spectra, absorption bands assigned to the C=N and C=C stretching

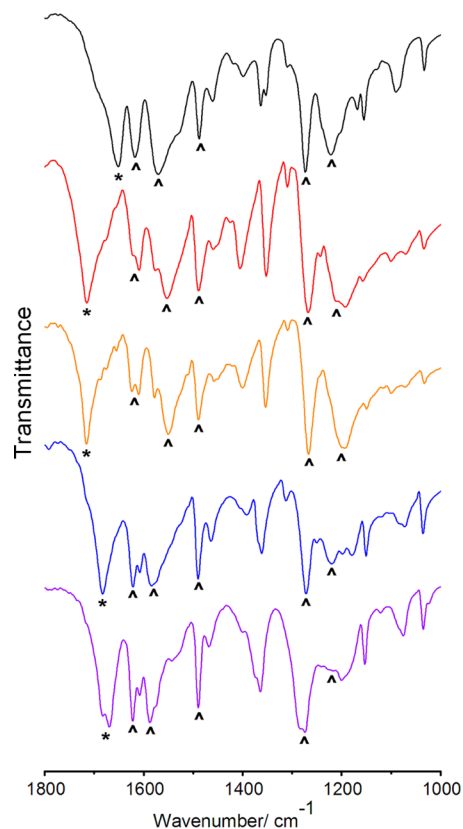
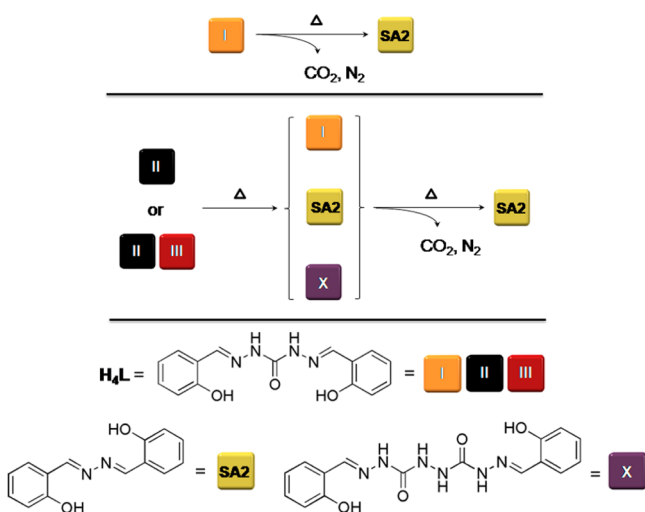


Figure 6. IR spectra of I (black), II (red), II/III mixture (orange), IV (blue), and V (violet) in the region $1800\text{--}1000\text{ cm}^{-1}$. Bands relevant for discussion are denoted with carets except amide I bands, which are denoted with asterisks.

modes appear at ca. 1620 and 1570 cm^{-1} , respectively. The N–H deformation mode (amide II band) occurs in all cases at ca. 1490 cm^{-1} , while bands corresponding to C(O)–N and C–O vibration modes appear at ca. 1270 and 1220 cm^{-1} , respectively.^{31a,32}

Thermal Behavior. Curious thermal behavior of carbonyl Schiff bases was documented as early as 1927 by Brown et al.^{33a} and later by Munro et al.,^{33b} who demonstrated that these compounds undergo complicated thermolyses, scenarios of which depend on the heating regime (Scheme S1, Supporting Information). According to the reports, when heated up to their melting points these Schiff bases underwent degradation, yielding as the final products corresponding azines and 4-aminourazole. However, the authors proposed that the degradation is in fact a two-stage process, proceeding via related hydrazidicarbonyl as an intermediate phase (for detailed discussion see Scheme S1 and Figure S19 in Supporting Information).

Thermogravimetric analysis (TGA) and differential scanning calorimetry (DSC) revealed complicated and divergent thermal behavior of polymorphs I–III (Scheme 2; Figures S20–S27 in Supporting Information). To inspect these in detail, thermal methods were coupled with powder X-ray diffraction and IR spectroscopy. According to the DSC curve, I does not display any thermal events upon heating up to a sharp endotherm at $222\text{ }^\circ\text{C}$ (onset, Figure S20a, Supporting Information). Although this event could be easily mistaken for melting of I, TGA revealed that this process is also accompanied by the sample's weight loss (Figure S20b,g, Supporting Information).

Scheme 2. Thermolyses of I–III^a

^aSA2, polymorphic form of salicylideneazine (SA); X, disalicylaldehydehydrazidicarbohydrazone.

Temperature-resolved powder X-ray diffraction (TR-PXRD) and additional TG/DSC experiments showed that, upon heating, I decomposes to salicylideneazine (SA) (more precisely SA2, according to TR-PXRD measurements; SA crystallizes in two polymorphic forms that are here denoted as SA1 and SA2; for detailed discussion see Figures S19–S21 in Supporting Information) as the only solid product and CO₂ and N₂ as the gaseous products, established upon TG-IR measurement (Scheme 2). Complete decomposition of I to SA2 (Figures S20 and S21, Supporting Information) was immediately followed, according both to the DSC and TR-PXRD experiments, by its melting giving rise to the sharp endotherm at 222 °C.

DSC curve of II indicated complicated transformations above 180 °C (Figure S22, Supporting Information). Several close endotherms were inspected by having five samples of II heated, each separately, from 170 to 195, 205, 210, 220, and 250 °C and then cooled to room temperature (Figure S23, Supporting Information), analyzed via PXRD, and inspected under the microscope. All samples heated below 220 °C contained large yellow needlelike single crystals of one of the salicylideneazine polymorphs (SA2). Upon heating up to 195 °C, II transformed partially to I and at the same time in part decomposed to salicylideneazine (according to DSC experiments coupled with PXRD, residues contained both SA1 and SA2), and an entirely new phase X (Figure S23a,b in Supporting Information; Scheme 2). Upon heating up to 205 °C, II completely disappeared and the resulting material contained I, SA2, and X, whereas the residue collected after heating to 210 °C was a mixture of X and SA2 (Figure S23c–f, Supporting Information). It is important to note that the above transformations occurred without considerable weight loss (at 210 °C, ca. 1.7%). Upon heating to even higher temperatures, X completely disappeared and the residues collected (220 and 250 °C) contained exclusively SA (220 °C residue was SA1, whereas the 250 °C residue was SA2; Figure S23g–j, Supporting Information). In contrast to processes occurring up to 210 °C, these were accompanied by significant weight loss (at 250 °C, ca. 11.8%); that is, the evolution of gaseous products CO₂ and N₂, established by TG-IR measurements. Phase X was identified via ESI-MS spectra acquired in both

positive and negative ion modes. On the basis of signals of protonated and sodiated molecule in the ESI-MS spectrum, observed at *m/z* 357.1 and 379.1, respectively, X was identified as disalicylaldehydehydrazidicarbohydrazone (Scheme 2), the same type of intermediate product postulated by Brown et al.^{33a} (Scheme S1 in Supporting Information; Scheme 2). In the course of TR-PXRD measurements of II, the first changes were detected at 200 °C by the simultaneous appearance of phases I and SA2 (Figure 7; Figure S24 in Supporting Information). As

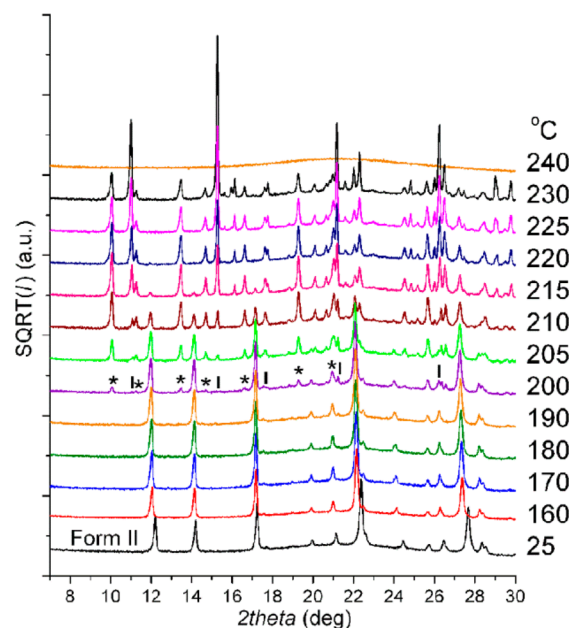


Figure 7. Powder patterns collected during heating of polymorph II. First changes are evident at 200 °C, where peaks of I and SA2 simultaneously appear. The peaks belonging to phase I are denoted with asterisks, whereas those corresponding to SA2 are designated with vertical bars. At 240 °C the sample had melted, as indicated by absence of diffraction peaks.

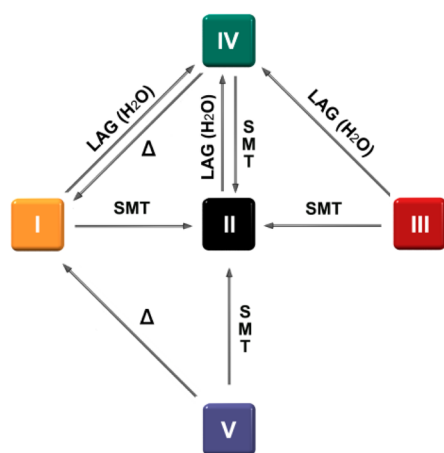
the temperature was further raised, the contributions of I and SA2 gradually increased on the account of the phase II. At ca. 220 °C, form II completely vanished, leaving I and SA2 as the only solid phases, while even further heating led to the progressive change of the sample's composition in favor of SA2 (Figure 7; Figure S24 in Supporting Information). Finally, at 240 °C the sample had melted. In the course of these measurements phase X was not detected, presumably due to its thermostability.

Complicated thermal behavior was established for the II/III mixture as well (Figure S25, Supporting Information). Samples of II/III were subjected to similar thermal treatment as II (Figure S26, Supporting Information). Analyses of the heating residues via PXRD, combined with visual inspection and TR-PXRD measurements (Figure 27), revealed that the II/III mixture first underwent partial transformation to I and thereafter formed a mixture of I, SA2, and X (Scheme 2; Figures S26 and S27 in Supporting Information). Similarly as in the case of II, these processes occurred without considerable weight loss (at 210 °C, ca. 1.7%). Upon further heating, I and X decomposed to CO₂ and N₂, leaving SA as the only solid product (220 °C heating residue was SA1, and that collected after heating up to 230 °C was SA2). These processes were accompanied by significant weight loss (at 230 °C, ca. 7.1%). It

is important to note that upon heating of II/III mixture, phase III was the first one to completely transform, while phase X was detected both by DSC/PXRD and TR-PXRD measurements (Figures S26 and S27, Supporting Information). Finally, it should be mentioned that in the course of the TR-PXRD measurements exclusively the SA2 form of salicylideneazine was detected, corroborating its thermodynamic stability. The occurrence of SA1 in some of the residues collected after heating might suggest that, during thermal rearrangements, some local melting of formed SA occurs. In such scenario, the appearance of SA1 or/and SA2 polymorphs would be associated with the serendipity of the crystallization event.

Solvates IV and V experience weight losses at 103 and 100 °C, respectively (onset, Figures S28 and S29, Supporting Information). These correspond to the loss of stoichiometric amounts of solvent molecules, water in IV and *tert*-butanol in V. Afterward, both samples display identical thermal behavior, which also resembles that of I. To inspect consequences of these thermal events, both samples were heated to 180 °C, cooled to room temperature, and subjected to PXRD. Powder patterns in both cases matched with that of I, revealing that under this heating regime both forms transform to I (Scheme 3; Figure S30 in Supporting Information).

Scheme 3. Transformations among Forms I–V^a



^aLAG, liquid-assisted grinding; SMT, solvent-mediated transition (MeOH). Δ denotes heating to 180 °C.

Mechanochemistry. Upon neat grinding (NG), forms I–III turned amorphous (Figure S31a–c, Supporting Information). IR spectra of materials obtained in this way were mutually identical but also matched the spectrum of form I (Figure S32, Supporting Information). NG treatment of I–III thus yielded a new amorphous phase in which molecules of H₄L have a similar environment as in phase I. Form IV proved resistant to mechanical force, confirmed by both PXRD and IR spectral data (Figures S31d and S32d, Supporting Information), whereas grinding of V for 40 min induced its partial conversion to I (Figure S31e, Supporting Information). LAG of I, II, and II/III mixture with water afforded without exception compound IV (Scheme 3; Figure S33 in Supporting Information).

Relative stability of the isolated phases was assessed via solvent-mediated experiments, which were conducted in methanol and revealed that at room temperature all forms convert to II (Scheme 3). In this particular collection of

polymorphs, form II can be considered as the thermodynamically stable one under the investigated conditions (Figure S11, Supporting Information).³⁴

NMR and UV Studies in Solution. Central fragment in carbohydrazone ligands can exist in both keto and enol tautomeric forms (Scheme S2a, Supporting Information). Keto–enol tautomeric interconversion can also involve the salicylidene part of the molecule since the hydroxyl group is situated in ortho position with respect to the C=N double bond. Furthermore, due to rotational flexibility around the central C–N linkage (N2–C8 or N3–C8; for numbering of atoms see Figure 2), in addition to *syn*, the *anti* isomers can exist as well (Scheme S2b, Supporting Information).^{7b,24a,35}

As discussed, in the solid state H₄L exists exclusively as a keto tautomer regarding carbamide and as an enol tautomer with respect to salicylidene fragment. This was also established as the most stable conformation in solution, as can be seen from NMR spectral data (Table 2). The ¹H and ¹³C chemical shifts

Table 2. ¹H and ¹³C NMR Chemical Shifts for H₄L in DMSO-*d*₆ at 20 °C

atoms ^a	δ _C , ppm	δ _H , ppm
1, 11	152.44	
2, 12	116.67	6.92
3, 13	128.65	7.26
4, 14	119.65	6.90
5, 15	128.47	7.71
6, 10	120.14	
7, 9	143.33	8.48
8	157.12	
N2H, N3H		10.86
O1H, O3H		10.86

^aFor atom numbering scheme, see Figure 2.

were determined by combined use of one-dimensional [¹H, ¹³C attached proton test (APT)] and two-dimensional [gradient-selected correlation spectroscopy (gCOSY), gradient-selected heteronuclear single quantum coherence (gHSQC), gradient-selected heteronuclear multiple bond correlation (gHMBC), and nuclear Overhauser effect spectroscopy (NOESY)] NMR techniques. The presence of the keto–enol tautomer was confirmed by chemical shifts and NOESY correlations between azomethine protons at 8.48 ppm and -NH protons at 10.86 ppm.

The signal at 10.86 ppm is due to -NH and -OH protons. Quite strong deshielding of these protons is the consequence of hydrogen-bond formation, which was confirmed by acquiring ¹H NMR spectra at different temperatures. The upfield shift of the signal at 10.86 ppm caused by an increase in temperature is characteristic for intramolecular hydrogen bonds. The signal at 8.48 ppm assigned to azomethine proton was not temperature-dependent, indicating that no *syn*–*anti* isomerization occurred. Although intramolecular H-bond formation was observed, no evidence of intramolecular proton transfer from oxygen to azomethine nitrogen and formation of keto tautomer was found. All carbon and proton chemical shift values indicate the presence of only one form in DMSO solution.

In Table 3 the UV spectral data of H₄L in protic and aprotic solvents of different polarities are shown. Due to possible hydrolysis of C=N double bond in solvents containing water, the spectra were acquired immediately after preparation of solutions. Bands in the spectral region 289–293 nm can be

Table 3. UV Spectral Data for H₄L in Solvents of Different Polarities

	λ , nm ($\epsilon \times 10^{-4}$ cm ⁻¹ ·mol ⁻¹ ·dm ³)				
chloroform	dimethyl sulfoxide	dimethyl formamide	dioxane	dioxane/water 1/1	methanol
not soluble	331 (2.70)	329 (2.96)	323 (2.17)	327 (2.67)	327 (2.72)
	292 (1.72)	293 (2.16)	289 (2.21)	293 (2.25)	291 (2.38)

assigned to the azomethine C=N bond and those at 323–331 nm to the salicylidene part of carbohydrazide, which was confirmed by acquiring the UV spectra of salicylaldehyde under the same experimental conditions. Since no solvent effects on UV spectra of H₄L were observed, no shifts of tautomeric equilibria should be expected.

DISCUSSION AND CONCLUSION

Depending on the synthetic approach, altogether five crystalline forms, three polymorphs (I–III) and two solvates (IV and V), of H₄L were obtained (Scheme 1). Solution synthesis was more suitable for preparation of I–III and V, while grinding proved to be superior for synthesis of IV. Among the solvents inspected, methanol was recognized as the most convenient for synthesis of I and II, and resolution between the two polymorphs was achieved by differing synthetic regimes. Recrystallization from aprotic solvents offered yet another route to II or IV. However, under the investigated conditions, it was not possible to isolate bulk sample of III, as it always appeared in concomitant mixtures with phase II at least.

Solid-state structures of I–IV were elucidated by combining SCXRD, CP MAS NMR, and IR spectral data, whereas the structure of V was deduced from the latter two. Molecules of H₄L within all five phases assume the same tautomeric form: enol-imino form regarding their salicylidene residues and keto form with respect to central carbamide fragments. Additionally, SCXRD analysis revealed that H₄L molecules in I–IV exist as syn isomers, and from comparison of CP MAS NMR and IR spectral data, the same can be proposed for V. As well, SCXRD analysis revealed a relationship between conformation of H₄L in polymorphs I–III and subsequent hydrogen-bonding pattern. Namely, if H₄L assumed a nearly planar conformation, as was the case in II and III, the central C8–O2 moiety was hindered and did not participate in hydrogen bonding. In contrast, deviation of H₄L from planarity, as seen in I, allowed the approach of N–H groups of the neighboring molecule and formation of R¹₂(6) hydrogen-bonding pattern with the central C8–O2 moiety. Although in IV the H₄L molecules adopt an essentially planar conformation, their central carbonyl groups realize hydrogen bonds but with smaller water molecules. Engagement of the C8–O2 group in hydrogen bonding was also evident from NMR and IR spectral data. From comparison of these data for I–IV on one hand and V on the other, it seems reasonable to suggest that the central carbonyl moiety of H₄L in V participates in hydrogen bonding. However, solely on the basis of these data it cannot be concluded with certainty whether hydrogen bonding includes neighboring H₄L molecules or rather *tert*-butanol ones.

Solution studies, namely NMR and UV spectroscopy, revealed that the same tautomeric form of H₄L found in the solid state is the predominant one in solution. The only apparent difference between solid-state and solution NMR spectra was the upfield shift of the imino-carbon (C-7,9; for numbering of atoms see Figure 2), which was attributed to formation of hydrogen bonds of the azomethine hydrogens with solvent (DMSO) molecules (Figure 5). Solution NMR

measurements clearly established that syn–anti isomerization and tautomeric conversion do not occur in DMSO solution. In addition, UV studies, which included several different solvents, have not revealed a shift of the tautomeric equilibria.

Properties and (inter)conversions of phases I–V were inspected via mechanochemistry, solvent-mediated experiments, and thermal analysis (Scheme 3). Neat grinding (NG) of I–III revealed existence of the new amorphous phase in which molecules, according to its IR spectra, have a similar local environment as in polymorph I. The same treatment (NG) has not induced any transformation for IV, while for V only partial conversion to I was established. On the other hand, LAG of I–III with water proved to be another elegant route to IV. Solvent-mediated experiments in methanol at room temperature revealed that forms I–V convert to II within a maximum of 32 h. Besides offering yet another approach to this phase, these results are important because they render, among the three polymorphs, II as the thermodynamically stable one at ambient conditions. Of especially high interest are the results of thermal analyses that combined TG/DSC measurements with TD-PXRD, IR spectroscopy, mass spectrometry, and visual inspection of the heating residues. A pioneering study on thermolyses of carbohydrazide Schiff bases was undertaken almost a century ago,³³ revealing that these compounds upon heating decompose to 4-aminourazole and the related azine via corresponding hydrazidicarbonylhydrazone as an intermediate phase. Compared to the above reports, this study established different thermal reactivity for salicylidene analogues. Referring in detail, it was revealed that form I upon heating undergoes direct decomposition mainly to CO₂, N₂ (in principle, water is also expected as a decomposition product), and solid salicylideneazine (SA), which afterward melts, giving rise to a sharp endotherm on the DSC curve (Scheme 2). However, since according to DSC no thermal events were observed before this endotherm, without additional measurements it might have been wrongly proclaimed as melting of I. On the other hand, conversion of I to SA was established prior to its melting, suggesting that the absence of a detectable DSC signal is most likely associated with small enthalpy change accompanying this process. In contrast to I, forms II and III undergo a different degradation pathway, first converting in part to I and in part decomposing to SA and disalicylaldehydrazidicarbonylhydrazone (X). Further heating induces decomposition of intermediates, I and X, to SA, CO₂, and N₂ (Scheme 2). It might be speculated that the differences in thermal behavior arise from diverse crystal structures of these forms, associated with different conformations of H₄L and hydrogen-bonding patterns. Forms IV and V, which are solvates, during heating (up to 180 °C) experience loss of solvent and yield form I, thus providing an alternative route to this phase.

In conclusion, this seemingly simple system afforded a wealth of solid forms, providing us with the prospect to study a number of related phenomena. Of special interest was the thermal behavior of compounds investigated herein, which differs appreciably from their analogues reported in the

literature, thus highlighting the influence of their parent aldehyde/ketone structure. On the other hand, this behavior was found to dramatically diverge between the polymorphs of the title compound, accentuating the intimate relationship between crystal architecture and properties of a compound. These topics, in our opinion, certainly deserve a detailed study, which should include a wide collection of carbonyl derivatives and will be addressed in our future investigations.

■ ASSOCIATED CONTENT

■ Supporting Information

Additional text, 32 figures, two tables, and two schemes with specific measurement details concerning solution NMR study; XRPD patterns of all isolated solid materials; detailed X-ray crystallography for solid forms I–IV (selected refinement data, selected geometrical parameters, and packing diagrams); details of thermal behavior of salicylideneazine (SA1 and SA2) and solid forms I–V (TG/SDTA, DSC, and TR-PXRD experiments); and IR spectra and PXRD patterns of materials obtained mechanochemically and by solvent-mediated experiments. This material is available free of charge via the Internet at <http://pubs.acs.org/>. CCDC reference numbers for compounds I–IV are 984038–984041.

■ AUTHOR INFORMATION

Corresponding Authors

*E-mail mirta@chem.pmf.hr.

*E-mail ngalic@chem.pmf.hr.

Notes

The authors declare no competing financial interest.

■ ACKNOWLEDGMENTS

This research was supported by the Ministry of Science, Education and Sports of the Republic of Croatia (Grants 119-1191342-1082, 119-1191342-1083, 119-1193079-1084, and 098-0982904-2953). We are grateful to Ljubica Ljubić and Dr. Jana Pisk for assistance concerning synthetic procedures and to Professor Marina Cindrić for critically reading the manuscript. We deeply appreciate fruitful discussions with Dr. Krunoslav Užarević. We are thankful to Professor R. E. Dinnebier for his support and help in the temperature-resolved powder diffraction experiment. N.J. thanks the ERASMUS 2013 program and Professor Augustin Curticeanu for providing the opportunity to perform evolved gas analysis.

■ REFERENCES

- (1) (a) Curtius, T.; Heidenreich, K. *Chem. Ber.* **1894**, *27*, 55–58. (b) Curtius, T.; Heidenreich, K. *J. Prakt. Chem.* **1895**, *52*, 454–489. (c) Mohr, E. B.; Brezinski, J. J.; Audrieth, L. F.; Ritchey, H. E.; McFarlin, R. F. In *Inorganic Syntheses*; Bailar, J. C., Jr., Ed.; McGraw-Hill Book Company Inc.: New York, 1953; Vol. IV, pp 32–35.
- (2) (a) Corwin, A. H.; Reinheimer, J. D. *J. Am. Chem. Soc.* **1951**, *73* (3), 1184–1186. (b) Audrieth, L. F.; Mohr, E. B.; Davis, E.; Tomlinson, W. R., Jr. In *Inorganic Syntheses*; Bailar, J. C., Jr., Ed.; McGraw-Hill Book Company Inc.: New York, 1953; Vol. IV, pp 29–32. (c) Audrieth, L. F.; Mohr, E. B. In *Inorganic Syntheses*; Bailar, J. C., Jr., Ed.; McGraw-Hill Book Company Inc.: New York, 1953; Vol. IV, pp 36–39. (d) Kurzer, F.; Wilkinson, M. *Chem. Rev.* **1970**, *70* (1), 111–149. (e) Kurzer, F.; Wilkinson, M. *J. Chem. Soc. C* **1970**, 19–25. (f) Kurzer, F. *J. Chem. Soc. C* **1971**, 2927–2931. (g) Kurzer, F.; Wilkinson, M. *J. Chem. Soc. C* **1970**, 26–34.
- (3) (a) Gordon, J. A.; Jencks, W. P. *Biochemistry* **1963**, *2* (1), 47–57. (b) Levine, L.; Gordon, J. A.; Jencks, W. P. *Biochemistry* **1963**, *2* (1), 168–175. (c) Pelttari, E.; Karhumäki, E.; Langshaw, J.; Elo, H. Z.

Naturforsch. **2007**, *62c*, 483–486. (d) Mansour, A. K.; Eid, M. M.; Khalil, N. S. A. M. *Molecules* **2003**, *8* (10), 744–755. (e) Dias, L. R. S.; Salvador, R. R. S. *Pharmaceuticals* **2012**, *5*, 317–324.

(4) Carbonylhydrazide was recognized as a superior alternative for oxygen scavenging in boiler systems than highly toxic and unstable hydrazine: (a) Buecker, B. *Power Plant Water Chemistry: A Practical Guide*; PenWell Publishing Co.: Tulsa, OK, 1997; pp 13–17. (b) Slovinsky, M. Boiler additives for oxygen scavenging. U.S. Patent 4,269,717, May 26, 1981. (c) Rudge, A.; Woosley, I. S.; Lewis, G. G.; Tyldesley, J. D. *Study of hydrazine alternatives under UK AGR plant operating conditions*; Proceedings of the Conference on Water Chemistry of Nuclear Reactor Systems 7, Bournemouth, U.K., October 13–17, 1996; British Nuclear Energy Society: London, 1996; Vol. 1, pp 399–406.

(5) (a) Užarević, K.; Đilović, I.; Matković-Čalogović, D.; Šišak, D.; Cindrić, M. *Angew. Chem., Int. Ed.* **2008**, *47*, 7022–7025. (b) Beer, P. D.; Gale, P. A. *Angew. Chem., Int. Ed.* **2001**, *40*, 486–516. (c) Užarević, K.; Đilović, I.; Bregović, N.; Tomišić, V.; Matković-Čalogović, D.; Cindrić, M. *Chem.—Eur. J.* **2011**, *17*, 10889–10897. (d) Užarević, K.; Halasz, I.; Đilović, I.; Bregović, N.; Rubčić, M.; Matković-Čalogović, D.; Tomišić, V. *Angew. Chem., Int. Ed.* **2013**, *52*, 5504–5508. (e) Sessler, J. L.; Roznyatovskiy, V.; Pantos, G. D.; Borisova, N. E.; Reshetova, M. D.; Lynch, V. M.; Khrustalev, V. N.; Ustynyuk, Y. A. *Org. Lett.* **2005**, *7* (23), 5277–5280.

(6) (a) Barragán de la Rosa, F. J.; Gómez Ariza, J. L.; Pino, F. *Mikrochim. Acta* **1984**, *82* (3–4), 171–182. (b) Gómez Ariza, J. L.; Barragán de la Rosa, F. J.; Montaña Gonzalez, M. T. *Mikrochim. Acta* **1984**, *83* (5–6), 407–416. (c) Rosales, D.; Gonzalez, G.; Gómez Ariza, J. L. *Talanta* **1985**, *32* (6), 467–474.

(7) (a) Stadler, A.-M.; Harrowfield, J. *Inorg. Chim. Acta* **2009**, *362*, 4298–4314. (b) Tandon, S. S.; Dul, M.-C.; Lee, J. L.; Dawe, L. N. M.; Anwar, U.; Thompson, L. K. *Dalton Trans.* **2011**, *40*, 3466–3475. (c) Hardy, J. G. *Chem. Soc. Rev.* **2013**, *42*, 7881–7899. (d) Manoj, E. P.; Kurup, M. R. P.; Fun, H.-K.; Punnoose, A. *Polyhedron* **2007**, *26*, 4451–4462. (e) Lozan, V.; Lassahn, P.-G.; Zhang, C.; Wu, B.; Janiak, C.; Rheinwald, G.; Lang, H. Z. *Naturforsch.* **2003**, *58b*, 1152–1164. (f) Manoj, E. P.; Kurup, M. R. P.; Fun, H.-K. *Inorg. Chem. Commun.* **2007**, *10*, 324–328.

(8) (a) Wöhler, F.; Liebig, J. *Ann. Pharm.* **1832**, 249–282. (b) David, W. I. F.; Shankland, K.; Pulham, C. R.; Blagden, N.; Davey, R. J.; Song, M. *Angew. Chem., Int. Ed.* **2005**, *44*, 7032–7035. (c) Thun, J.; Seyfarth, L.; Senker, J.; Dinnebier, R. E.; Breu, J. *Angew. Chem., Int. Ed.* **2007**, *46*, 6729–6731. (d) Ostwald, W. Z. *Phys. Chem.* **1897**, *22*, 289–330. (e) Bernstein, J. *Polymorphism in Molecular Crystals*, 1st ed.; Oxford University Press Inc.: New York, 2002. (f) Bernstein, J. *Cryst. Growth Des.* **2011**, *11* (3), 632–650. (g) Dunitz, J.; Bernstein, J. *Acc. Chem. Res.* **1995**, *28*, 193–200. (h) Vippagunta, S. R.; Brittain, H. G.; Grant, D. J. W. *Adv. Drug Delivery Rev.* **2001**, *48*, 3–26. (i) Threlfall, T. L. *Analyst* **1995**, *120*, 2435–2460. (j) Guillory, J. In *Polymorphism in Pharmaceutical Solids*; Brittain, H., Ed.; Marcel Dekker: New York, 1999; Vol. 95, pp 183–226.

(9) (a) Braga, D.; Bernstein, J. In *Making Crystals by Design: Methods, Techniques and Applications*; Braga, D., Grepioni, F., Eds.; Wiley-VCH Verlag GmbH & Co. KGaA: Weinheim, Germany, 2007; Chapt. 3.3, pp 293–314. (b) McCrone, W. C. In *Physics and Chemistry of the Organic Solid State*; Fox, D., Labes, M. M., Weissberger, A., Eds.; Interscience Publishers: New York, 1965; Vol. 2, pp 725–767. (c) Stahly, G. P. *Cryst. Growth Des.* **2007**, *7* (6), 1007–1026. (d) Llinàs, A.; Goodman, J. M. *Drug Discovery Today* **2008**, *13* (5–6), 198–210. (e) Datta, S.; Grant, D. J. W. *Nat. Rev.* **2004**, *3*, 42–57. (f) Snider, D. A.; Addicks, W.; Owens, W. *Adv. Drug Delivery Rev.* **2004**, *56*, 391–395. (g) Hancock, B. C.; Zografi, G. *J. Pharm. Sci.* **1997**, *86*, 1–12.

(10) (a) Aakeröy, C. B.; Nieuwenhuyzen, M.; Price, S. L. *J. Am. Chem. Soc.* **1998**, *120*, 8986–8993. (b) Braga, D.; Grepioni, F.; Dyson, P. J.; Johnson, B. F. G.; Frediani, P.; Bianchi, M.; Piacenti, F. *J. Chem. Soc., Dalton Trans.* **1992**, 2565–2571. (c) Aakeröy, C. B.; Beatty, A. M.; Helfrich, B. A.; Nieuwenhuyzen, M. *Cryst. Growth Des.* **2003**, *3* (2), 159–165. (d) Braga, D.; Grepioni, F.; Maini, L.; Polito, M. In *Structure and Bonding, Molecular Networks*; Hosseini, M. W., Ed.;

Springer-Verlag: Berlin and Heidelberg, 2009; Vol. 132, pp 25–50. (e) Senthil Kumar, V. S.; Sheela, K. C.; Nair, V.; Rath, N. P. *Cryst. Growth Des.* **2004**, *4* (6), 1245–1247. (f) Rath, N. P.; Kumar, V. S. S.; Janka, M.; Anderson, G. K. *Inorg. Chim. Acta* **2007**, *360*, 2997–3001. (g) Nangia, A. *Acc. Chem. Res.* **2008**, *41*, 595–604. (h) Davey, D. R. J.; Blagden, N.; Potts, G. D.; Docherty, R. J. *Am. Chem. Soc.* **1997**, *119*, 1767–1772. (i) Yu, L. *Acc. Chem. Res.* **2010**, *43* (9), 1257–1266. (j) Rubčić, M.; Milić, D.; Pavlović, G.; Cindrić, M. *Cryst. Growth Des.* **2011**, *11* (12), 5227–5240.

(11) Schmidt, G. M. J. *J. Chem. Soc.* **1964**, 2014–2021.

(12) (a) Zhimin, H.; Iqbal, A. *Chem. Soc. Rev.* **1997**, *26*, 203–213.

(b) Hunger, K. *Rev. Prog. Color. Relat. Top.* **1999**, *29*, 71–84.

(c) Deschamps, J. R.; Parrish, D. A.; Butcher, R. J. *NRL Rev.* **2008**, 71–77.

(13) Bauer, J.; Spanton, S.; Henry, R.; Quick, J.; Dziki, W.; Porter, W.; Morris, J. *Pharm. Res.* **2001**, *18* (6), 859–866.

(14) Among other approaches, we have also inspected the influence of an additive on the crystallization outcome. Since our previous studies demonstrated that the use of 4,4'-bipy (as an additive) can be beneficial in terms of selective polymorph crystallization (ref 28k), we employed the same compound here. It is worth noting that in this particular case 4,4'-bipy had a 2-fold role. On one hand, it directed crystallization of pure form I, but at the same time it facilitated the formation of fine-quality crystals, crucial for single-crystal X-ray diffraction experiments, which we had severe difficulties in obtaining otherwise.

(15) Xcalibur CCD system: CrysAlis Software system, versions 1.171.33.66, 1.171.34.44, and 1.171.36.28; Oxford Diffraction Ltd.: Abingdon, Oxfordshire, U.K., 2008.

(16) Sheldrick, G. M. *Acta Crystallogr., Sect. A* **2008**, *64*, 112–122.

(17) Farrugia, L. J. *J. Appl. Crystallogr.* **1999**, *32*, 837–838.

(18) Spek, L. J. *J. Appl. Crystallogr.* **2003**, *36*, 7–13.

(19) (a) Nardelli, M. *Comput. Chem.* **1983**, *7*, 95–98. (b) Nardelli, M. *J. Appl. Crystallogr.* **1995**, *28*, 659–673.

(20) Farrugia, L. J. *J. Appl. Crystallogr.* **1997**, *30*, 565.

(21) <http://www.povray.org/>.

(22) Macrae, C. F.; Bruno, I. J.; Chisholm, J. A.; Edgington, P. R.; McCabe, P.; Pidcock, E.; Rodriguez-Monge, L.; Taylor, R.; van de Streek, J.; Wood, P. A. *J. Appl. Crystallogr.* **2008**, *41*, 466–470.

(23) (a) Dutta, R. L.; Hossain, M. M. *Indian J. Chem.* **1983**, *22A*, 201–203. (b) Dan, J.; Seth, S.; Chakraborty, S. *Acta Crystallogr., Sect. C* **1987**, *43*, 1114–1116.

(24) (a) Bustos, C.; Burckhardt, O.; Schrebler, R.; Carrillo, D.; Arif, A. M.; Cowley, A. H.; Nunn, C. M. *Inorg. Chem.* **1990**, *29*, 3996–4001. (b) Kogan, V. A.; Lukov, V. V.; Novotortsev, V. M.; Eremenko, I. L.; Aleksandrov, G. G. *Russ. Chem. Bull., Int. Ed.* **2005**, *54* (3), 600–605. (c) Affan, M. A.; Liew, Y. Z.; Ahmad, F. B.; Shamsuddin, M. B.; Yamin, B. M. *Indian J. Chem.* **2007**, *46A*, 1063–1068. (d) Li, Z.; Zhu, W.; Yu, J.; Ma, X.; Lu, Z.; Xiao, S. *Synth. Commun.* **2006**, *36* (18), 2613–2619.

(25) Bikas, R.; Anarjan, P. M.; Weng Ng, S.; Tiekink, E. R. T. *Acta Crystallogr., Sect. E* **2012**, *68*, o413–o414.

(26) The structures of the two forms reported (here named II and IV) were previously elucidated. We undertook new refinements as in the case of II (ref 25): data were collected at low temperature. Since we conducted this study mostly referring to room temperature (or higher temperatures), we considered it important to have structural models of all phases at room temperature. In the case of IV (ref 23b), the previous structural model was incomplete, since it was missing the N–H/O–H hydrogen atoms. Since this study, among other, addresses hydrogen bonding in the solid state, we considered it essential to have complete structural models.

(27) Novak, P.; Jednačak, T.; Parlov Vuković, J.; Zangger, K.; Rubčić, M.; Galić, N.; Hrenar, T. *Croat. Chem. Acta* **2012**, *85* (4), 451–456.

(28) (a) James, S. L.; Adams, C. J.; Bolm, C.; Braga, D.; Collier, P.; Friščić, T.; Grepioni, F.; Harris, K. D.; Hyett, G.; Jones, W.; Krebs, A.; Mack, J.; Maini, L.; Orpen, A. G.; Parkin, I. P.; Shearouse, W. C.; Steed, J. W.; Waddell, D. C. *Chem. Soc. Rev.* **2012**, *41* (1), 413–447. (b) Friščić, T. *Chem. Soc. Rev.* **2012**, *41*, 3493–3510. (c) Aakeröy, C. B.; Chopade, P. D. *Org. Lett.* **2011**, *13* (1), 1–3. (d) Štrukil, V.; Igrc,

M. D.; Eckert-Maksić, M.; Friščić, T. *Chem.—Eur. J.* **2012**, *18*, 8464–8473. (e) Braga, D.; Maini, L.; Grepioni, F. *Chem. Commun.* **1999**, 937–938. (f) Bučar, D.-K.; Filip, S.; Arhangelskis, M.; Lloyd, G. O.; Jones, W. *CrystEngComm* **2013**, *15*, 6289–6291. (g) Friščić, T.; Trask, A. V.; Jones, W.; Motherwel, W. D. S. *Angew. Chem., Int. Ed.* **2006**, *45*, 7546–7550. (h) Užarević, K.; Rubčić, M.; Radić, M.; Puškarić, A.; Cindrić, M. *CrystEngComm* **2011**, *13*, 4314–4323. (i) Braga, D.; Giaffreda, S. L.; Grepioni, F.; Polito, M. *CrystEngComm* **2004**, *6* (75), 458–462. (j) Cindrić, M.; Uzelac, M.; Cinčić, D.; Halasz, I.; Pavlović, G.; Hrenar, T.; Ćurić, M.; Kovačević, D. *CrystEngComm* **2012**, *14*, 3039–3045. (k) Užarević, K.; Rubčić, M.; Đilović, I.; Kokan, Z.; Matković-Čalogović, D.; Cindrić, M. *Cryst. Growth Des.* **2009**, *9* (12), 5327–5333.

(29) (a) Castellani, F.; van Rossum, B.; Diehl, A.; Schubert, M.; Rehbein, K.; Oschkinat, H. *Nature* **2002**, *420*, 98–102. (b) Zumbulyadis, N.; Antalek, B.; Windig, W.; Scaringe, R. P.; Lanzafame, A. M.; Blanton, T.; Helber, M. *J. Am. Chem. Soc.* **1999**, *121*, 11554–11557. (c) Berendt, R. T.; Sperger, D. M.; Munson, E. J.; Isbester, P. K. *Trends Anal. Chem.* **2006**, *25* (10), 977–984. (d) Conte, P.; Spaccini, R.; Piccolo, A. *Prog. Nucl. Magn. Reson. Spectrosc.* **2004**, *44*, 215–223. (e) Etter, M. C.; Hoye, R. C.; Vojta, G. M. *Cryst. Rev.* **1988**, *1* (4), 281–333.

(30) (a) Claramunt, R. M.; López, C.; Santa María, M. D.; Sanz, D.; Elguero, J. *Prog. Nucl. Magn. Reson. Spectrosc.* **2006**, *49*, 169–206. (b) Makal, A.; Schilf, W.; Kamiński, B.; Szady-Chelminiecka, A.; Grech, E.; Wóznik, K. *Dalton Trans.* **2011**, *40*, 421–430. (c) Rubčić, M.; Užarević, K.; Halasz, I.; Bregović, N.; Mališ, M.; Đilović, I.; Kokan, Z.; Stein, R. S.; Dinnebier, R. E.; Tomišić, V. *Chem.—Eur. J.* **2012**, *18*, 5620–5631. (d) Rozwadowski, Z.; Dziembowska, T. *Magn. Reson. Chem.* **1999**, *37*, 274–278. (e) Dziembowska, T.; Szafran, M.; Katrusiak, A.; Rozwadowski, Z. *J. Mol. Struct.* **2009**, *929*, 32–42. (f) Domínguez, O.; Rodríguez-Molina, B.; Rodríguez, M.; Ariza, A.; Farfán, N.; Santillan, R. *New J. Chem.* **2011**, *35*, 156–164. (g) Jaworska, M.; Hryncyszyn, P. B.; Welniak, M.; Wojtczak, A.; Nowicka, K.; Krasinski, G.; Kassassir, H.; Ciesielski, W.; Potrzebowski, M. *J. Phys. Chem. A* **2010**, *114*, 12522–12530. (h) Schilf, W.; Kamiński, B.; Užarević, K. *J. Mol. Struct.* **2013**, *1031* (16), 211–215.

(31) (a) Pretsch, E.; Bühlmann, P.; Affolter, C. In *Structure Determination of Organic Compounds: Tables of Spectral Data*; Pretsch, E., Bühlmann, P., Affolter, C., Eds.; Springer-Verlag: Berlin and Heidelberg, 2000. (b) Kolodziejski, W.; Wawer, I.; Wozniak, K.; Klinowski, J. *J. Phys. Chem.* **1993**, *97*, 12147–12152. (c) Etter, M. C.; Urbakzyk-Lipkowska, Z.; Zia-Ebrahimi, M.; Panunto, T. W. *J. Am. Chem. Soc.* **1990**, *112*, 8415–8426. (d) Macholl, S.; Börner, F.; Buntkowsky, G. *Chem.—Eur. J.* **2004**, *10*, 4808–4816.

(32) Escobar Godoy, R.; Barragán de la Rosa, F. J.; Gómez Ariza, J. L. *J. Mol. Struct.* **1986**, *143*, 505–508.

(33) (a) Brown, A. C.; Pickering, E. C.; Wilson, F. J. *J. Chem. Soc.* **1927**, 107–112. (b) Munro, A. M.; Wilson, F. J. *J. Chem. Soc.* **1928**, 1257–1261.

(34) Stability order among polymorphs can be deduced in several ways. One of the simple approaches, the density rule, compares the densities of the polymorphs, considering that the polymorph of the highest density is the most stable one. [For a detailed discussion on the density rule, see (a) Burger, A.; Ramberger, R. *Mikrochim. Acta* **1979**, *II*, 259–272. (b) Burger, A.; Ramberger, R. *Mikrochim. Acta* **1979**, *II*, 273–316 and ref 8e.] Although this rule applies well in 90% of cases, discrepancies may arise when interactions such as hydrogen bonding govern the packing. These can in some cases lead to molecular arrangements that leave voids in the structure, subsequently lowering the density of the material. When such ambiguities arise, it is advisable to compare the conclusion based on the density rule against the results deduced via another approach, such as solvent-mediated transition experiment (SMT; see for example ref 9c). Typically, the procedure involves suspending the mixture of polymorphs at a chosen temperature in a solvent that is saturated with the investigated compound. The resulting slurry is subsequently stirred and the more stable polymorph, at a given temperature, should be the only remaining phase after a certain period of time. When both approaches

were tested on the herein-investigated system (under the same ambient conditions), the density rule would imply **III** > **II** > **I** stability order of the polymorphs, whereas the SMT experiments clearly establish polymorph **II** as the stable one. Although the packing modes in **II** and **III** are fairly similar, considering the conformation of molecules and primary hydrogen-bonding motifs, some differences are nevertheless observed, for example, in C–H... π interactions.

(35) (a) Chandra, S.; Sharma, A. K. *Spectrochim. Acta, Part A* **2009**, *72*, 851–857. (b) Bacchi, A.; Carcelli, M.; Pelagatti, P.; Pelizzi, C.; Pelizzi, G.; Zani, F. *J. Inorg. Biochem.* **1999**, *75*, 123–133. (c) Galić, N.; Brođanac, I.; Kontrec, D.; Miljanić, S. *Spectrochim. Acta, Part A* **2013**, *107*, 263–270. (d) Galić, N.; Dijanošić, A.; Kontrec, D.; Miljanić, S. *Spectrochim. Acta, Part A* **2012**, *95*, 347–353. (e) Galić, N.; Rubčić, M.; Magdić, K.; Cindrić, M.; Tomišić, V. *Inorg. Chim. Acta* **2011**, *366*, 98–104.